ISSN 1392 - 1207. MECHANIKA. 2011. 17(2): 149-155

Numerical investigation of thermo-fluid dynamics of two triangular jets

I. Chitsaz*, B. Farhanieh**
**School of Mechanical Engineering, Sharif University of Technology, Tehran, Iran, E-mail: i_chitsaz@mech.sharif.ir*
***School of Mechanical Engineering, Sharif University of Technology, Tehran, Iran, E-mail: bifa@sharif.ir*

crossref http://dx.doi.org/10.5755/j01.mech.17.2.330

1. Introduction

Free jets represent a very good benchmark for research in the physics of turbulent fluid flow. Numerical and experimental investigations of planar, circular, rectangular and elliptic jets have been widely studied [1-3]. Good mixing characteristics of noncircular jets increased the attention of researchers to these types of jets. Among the various types of noncircular jets, the triangular jet was extensively studied because many engineering systems can be accommodated into this configuration. Typical examples include internal combustion engines, propulsion, spray driers, laser machining of metals, mixing of chemical reactants, cooling of blades and others.

Xu and Antonia [4] examined axisymmetric nozzles' jet flow configurations and observed that there was slight improvement in fluid entrainment and jet spreading rates of the circular nozzle as compared to the fully developed turbulent jet pipe flow. Recent studies showed an immense increase in entrainment rate of asymmetric nozzles. Asymmetric nozzles promote higher entrainment and jet spreading compared to their circular counterparts [4-7]. Mi et al [4] experimentally studied nine nozzle shapes of circular and noncircular jets. They investigated the mean and fluctuations of centerline velocity at a Reynolds number of 1.5×10^4. It is mentioned that the triangular nozzle's jet has a higher entrainment rate than the rectangular jet [7]. Quinn [7] covered out experimental investigation of isosceles triangular jet and showed that it has the best mixing enhancement characteristics among noncircular turbulent jets. Mean streamwise velocity and static pressure distribution on the jet centerline of the isosceles triangular jet were obtained. All measurements were performed at Reynolds number of 1.84×10^5. Schadow et al [8] experimentally investigated the exhaust nozzles with sharp corners (triangular exit cross-sections) for the purpose of passive shear-flow control. One of the advantages of sharp-edged non-circular geometries, such as the triangular nozzle, is that large-scale turbulence is generated along the sides of the nozzle, while small-scale turbulence is generated at the vertices. Miller et al [9] studied noncircular jets numerically using direct numerical simulation. They investigated the fluid dynamics of the flow field and combustion of a variety of noncircular jets at low specified Reynolds number. The jets were discharged to a nonstagnant ambient. Influence of jet cross-section on the flow and combustion were studied and showed that the triangular jets have higher mixing ability compared with the other noncircular jets. Quinn [10] experimentally studied a triangular cross-section free jet and presented the contours of average and fluctuating velocity component.

In the present research numerical investigation of two interacting triangular jets, using two equation turbulence models is considered. Effects of vertex angle, Reynolds number and distance between jets on mixing parameters and potential core lengths, have been studied. Numerical simulations were validated with experimental results for a single three dimensional triangular jet. Due to their robustness and efficiency eddy viscosity models (EVM) are used widely to predict practical turbulent flow [11] and the most popular EVM is the $k-\varepsilon$ models. $k-\varepsilon$ models have been widely used to predict turbulent flow due to their simplicity and lower computational cost in comparison with RSM and LES. Benhamza and Belaid [12] also used the eddy viscosity model for their simulation. Despite significant developments in the measurement techniques and instrumentation, as well as in the numerical methods with improved computing capacity, the study of two jets in triangular geometry has not been reported yet. The objective of this paper is to fill this gap by performing numerical simulations and reports an investigation of the influence of inflow condition of triangular nozzles on the properties of a triangular jets discharging into a large space. Another issue, which has to be emphasized, is that the temperature field was investigated too. The validation of the numerical code was performed by comparing velocity profiles against experimental measurements and satisfactory agreement was observed. The region under consideration spans the near- and far-fields, $0 < x / D_e < 100$. Thermo-fluid dynamics fields are studied using streamlines and contours of velocity and temperature. In sections 2 and 3 mathematical and numerical formulations are presented. Results of simulation are outlined in section 4, 5.

2. Mathematical models

In the present study, it is assumed that the fluid is incompressible and Newtonian with temperature-independent fluid properties. A numerical solution of the mean flow and thermal fields requires resolving the continuity equation; Reynolds averaged Navier–Stokes equation and time-averaged energy equation

$$\frac{\partial \overline{u}_i}{\partial x_i} = 0 \tag{1}$$

$$\rho\left(\frac{\partial \overline{u_i}}{\partial t} + \overline{u}_j \frac{\partial \overline{u_i}}{\partial x_j}\right) = -\frac{\partial P}{\partial x_i} + \frac{\partial}{\partial x_j}\left(\mu\left(\frac{\overline{\partial u_i}}{\partial x_j} + \frac{\overline{\partial u_j}}{\partial x_i}\right) - \rho\overline{u_i' u_j'}\right) \tag{2}$$

$$\rho c_p \overline{u}_i \frac{\partial \overline{T}}{\partial x_i} = \frac{\partial}{\partial x_i}\left(k\frac{\partial \overline{T}}{\partial x_i} - \rho\overline{u_i' T'}\right) \tag{3}$$

As it shown in equation (2) and (3), additional term $-\rho\overline{u_i'u_j'}$ and $\rho\overline{u_i'T'}$ was entered in energy and Navier-Stokes equations. Additional terms should be modeled. Boussinesq represent a fundamental equation that is shown in Eq. (4). Some of turbulence models such as $k-\varepsilon$ use this fundamental equation

$$\rho\overline{u_i'u_j'} = -\mu_t\left(\frac{\partial \bar{u}_i}{\partial x_j}+\frac{\partial \bar{u}_j}{\partial x_i}\right)+\frac{2}{3}\rho k\delta_{ij} \tag{4}$$

In Boussinesq approximation, the Reynolds stress is related to the local velocity gradients introducing the eddy viscosity υ_t. The turbulence scalar quantities (k and ε) used to calculate υ_t are determined from the following modelled transport equations

$$\frac{\partial}{\partial x_j}\left(\rho \bar{u}_j k\right)=\frac{\partial}{\partial x_j}\left(\frac{\mu_{eff}}{\sigma_k}\frac{\partial k}{\partial x_j}\right)+$$
$$\mu_t\left(\frac{\partial \bar{u}_j}{\partial x_i}+\frac{\partial \bar{u}_i}{\partial x_j}\right)\frac{\partial \bar{u}_i}{\partial x_j}-\rho\varepsilon \tag{5}$$

$$\frac{\partial}{\partial x_j}\left(\rho \bar{u}_j \varepsilon\right)=\frac{\partial}{\partial x_j}\left(\frac{\mu_{eff}}{\sigma_\varepsilon}\frac{\partial \varepsilon}{\partial x_j}\right)+$$
$$+c_1\frac{\varepsilon}{k}\mu_t\left(\frac{\partial \bar{u}_j}{\partial x_i}+\frac{\partial \bar{u}_i}{\partial x_j}\right)\frac{\partial \bar{u}_i}{\partial x_j}-c_2\frac{\varepsilon^2}{k}\rho \tag{6}$$

$$\mu_t = c_\mu\rho\frac{k^2}{\varepsilon} \tag{7}$$

$$\mu_{eff} = \mu_t+\mu \tag{8}$$

$$\overline{u_i'T'} = -\alpha_i\left(\frac{\partial T}{\partial x_i}\right),\quad \alpha_t=\frac{c_\mu}{Pr_t}\frac{k^2}{\varepsilon} \tag{9}$$

where $C_\mu, C_1, C_2, \sigma_k$ and σ_ε are empirical turbulence model constants those cited in Table 1.

Table 1
Model constants in $k-\varepsilon$ turbulence model [13]

Constant	σ_ε	σ_k	c_μ	c_2	c_1
Value	1.3	1.0	0.09	1.92	1.44

Two dimensionless parameters that control the characteristics of flow field and performance of jets are Reynolds number and discharging moment at the inlet of jet. Discharging momentum is introduced in to Eq. (10) and simplified in Eq. (11)

$$J_{in} = \int\rho\vec{V}(\vec{V}\,d\,\vec{A}) \tag{10}$$

After simplification, the above equation is converted to Eq. (11)

$$J_{in} = \frac{\pi}{4}\frac{\mu^2}{\rho}Re_D^2 \tag{11}$$

3. Numerical simulations

Transport equation for variable ϕ in Cartesian coordinate is written as

$$\frac{\partial}{\partial t}(\rho\phi)+\frac{\partial}{\partial x_i}(\rho U_i\phi)=\frac{\partial}{\partial x_i}\left(\Gamma_\phi\frac{\partial\phi}{\partial x_i}\right)+S \tag{12}$$

In the above equation Γ_ϕ is diffusion coefficient and represent viscosity and thermal diffusivity in momentum and energy equation, respectively. The nonuniform collocated grid was used with the SIMPLEC [14] algorithm to correct the velocity field and to calculate the pressure field. Rhie-Chow interpolation [15] is used to prevent pressure field oscillations. Diffusion terms are discretized with the central differencing scheme. Van Leer [16] and QUICK [17] scheme is adopted for the convective terms in the momentum and energy equations. Discretized equations are solved iteratively using tridiagonal matrix algorithm. Convergence criterion is based on the sum of absolute residuals divided by the inlet fluxes. The residual in convergence state is in order of 10^{-5}. Schematic of considered geometry is shown in Fig. 1. Due to the existence of strong velocity gradients around jets centerline, a nonuniform mesh of $120\times90\times80$ is used for simulation of the flow. The considered grid is shown in Fig. 2.

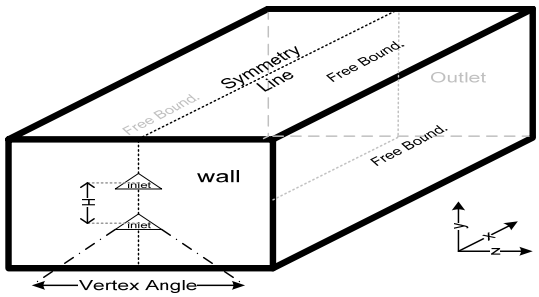

Fig. 1 schematic of the geometry

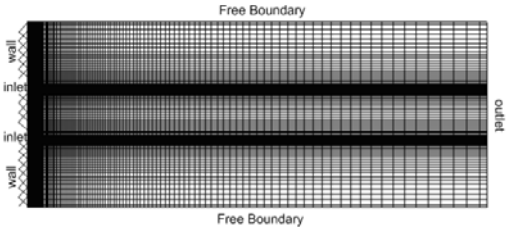

Fig. 2 Adopted mesh and boundary conditions at symmetry plane

4. Results and discussion

There is no comparable experimental or numerical past data for the present study on turbulent triangular jets. The solution procedure has been validated using a set of experiment data of the triangular jet (Mi et al. and Quinn) those selected from available literature and compared with results of numerical simulation. Fig. 3 shows a comparison of centerline velocity of equilateral triangular jet predicted by $k-\varepsilon$ models with experimental data [7] at Reynolds number of 184000. As Shown in Fig. 3 that numerical simulation estimated the shape of the centerline velocity profile quite well, but overestimated the magni-

tudes of velocity at both near and farfield. As it can be seen, there is good agreement between analytical and numerical simulation in the farfield region.

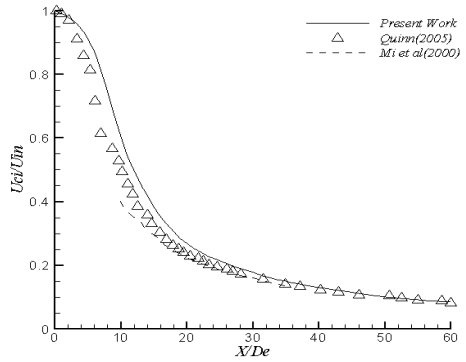

Fig. 3 Comparison of experimental and numerical solution for equilateral triangular jet

The decay rate of mean streamwise velocity in the near flow field is presented in Fig. 4 to shed some light on the nearfield mixing characteristics of the jets. The $k-\varepsilon$ model performs worse prediction of the nearfield than the farfield. In the nearfield region, rapid production of turbulence and changing velocity occurs; therefore the overestimation of centerline velocity is predictable. The near flow field is a region of interest in practical jet applications, such as in combustion. The length of the potential core, among other parameters, is a better indicator of near field mixing effectiveness in a jet. The potential core lengths of isosceles and equilateral triangular jet in the present study are $3.27D_e$, $3.1D_e$, respectively. The potential core lengths in the experiment [7] are $2.91D_e$, $3.14D_e$ and $3.50D_e$ for the equilateral triangular jet, isosceles triangular jet and round jet, respectively.

Due to geometrical and physical symmetry, only the flow field within the half domain shown in Fig. 1 was solved numerically. Free boundaries at the outlet flow,

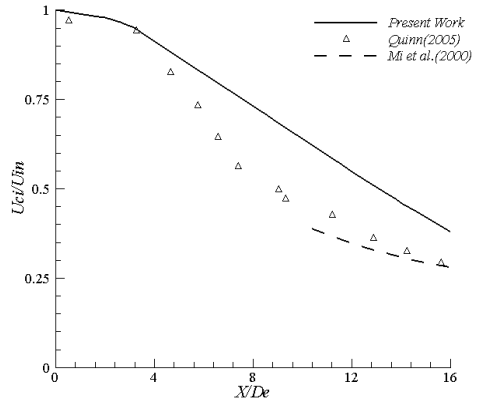

Fig. 4 Near field mean streamwise velocity decay on the jet centreline

those are not in the streamwise, should be located at 15 times of hydraulic diameter outer from centerline of jet. Outlet of streamwise is located 100 times of hydraulic diameter far from centerline of jet [18, 19]. All jets in this study have 0.1 m hydraulic diameter. Boundary conditions for temperature equation are 298 K for ambient and temperature of jet is 392 K .The grid independency is performed for all simulations. Grid independency for centerline of upper jet is shown in Fig. 5. As it is shown in Fig. 5 by using more coarse mesh, result changes and the best independent mesh is $100\times80\times70$.

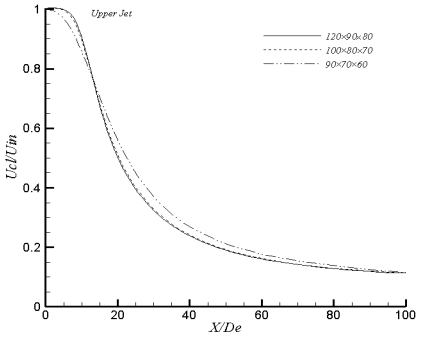

Fig. 5 Grid independency of numerical solution

The structure of the solution at the $Re=5000$, $J_{in}=0.0392$ and equilateral triangular jets with the same hydraulic diameter with $H=10\,D_e$, are given in Fig. 6, which shows the velocity vectors at the symmetry plane. The flow entrainment from free boundaries to the main jet can be seen clearly in this figure. It is evident from the magnitude of the velocity vectors that gradient is the highest near the inlet of jets and resulting high production of turbulence, which is then, diffused from the shear layers to the jet centerline. The higher streamwise turbulence intensity values in the triangular jet flow, in the initial region, provide further evidence of better near-field mixing in the triangular jets.

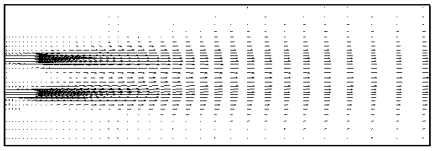

Fig. 6 velocity vectors at symmetry plane

The dimensionless velocity and temperature contours at symmetry plane are presented in Figs. 7 and 8, respectively. The contours of the velocity field indicate how the jet spreads due to the strong shear layer effects. The change of flow near the edge of jet is representative of intense gradient there, which is the reason of jets spread at unbounded domain. The temperature contours illustrate the decrease of the jet temperature approaches to ambient temperature at farther locations. It is obvious from Figs. 7 and 8 that centerline temperature of the jets decays more rapidly than velocity. The transversal flow vectors at downstream location are shown in Fig. 9. Vectors of the mean spanwise and lateral velocity shown in Fig. 9, describe how secondary flow pattern, in the near and farfield, is made up. This field shows the mass transfer from free boundaries toward the jet. Having strong shear stresses on the jet edges, another flow is inducted from the jet center toward its edges that accelerates the jet spread in the infinite ambient. The base-side spreading leads to an inversion of the shape of the jet at the downstream of jets. Moving along the *x*-direction, the triangular jets will turn into a circular one.

Fig. 7 Dimensionless velocity contours at symmetry plane

Fig. 8 Dimensionless temperature contours at symmetry plane

The combined effect of the spanwise and lateral secondary flow is consistent with the faster spreading of jets on its base side, as noted earlier. Mass entrainment from the free boundaries to the main stream jet can be seen in these figures. As a result of shear stresses, a radial flow is formed from jet centerline to its edge, causing the expansion of the jet while moving downstream. Thus the flow rate increases. The centerline normalized velocity and the temperature decay curves along the centerline of upper jet plotted in Fig. 10. It can be seen from this figure that close to the nozzle the velocity and temperature possess a constant value and further downstream their values decrease sharply over a short distance.

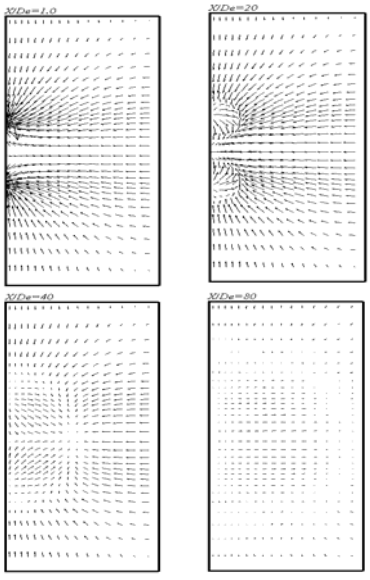

Fig. 9 Cross stream flow field at some X / D_e

The potential core length of lower and upper jet is respectively equal to 2.75 and 2.57. In general, relative to the one triangular jet; the centreline mean velocity of the two jets decays more rapidly, implying increased entrainment of ambient fluid. The initial turbulence level is the highest at the triangle's vertices [20]. Consequently, due to smaller distance of lower jet centerline to the corners of upper and lower jet its potential core decreases. The shorter potential core length of the jets indicates better near-field mixing. Interaction between jets increases fine-scale mixing, which is important for efficient chemical reactions including combustion.

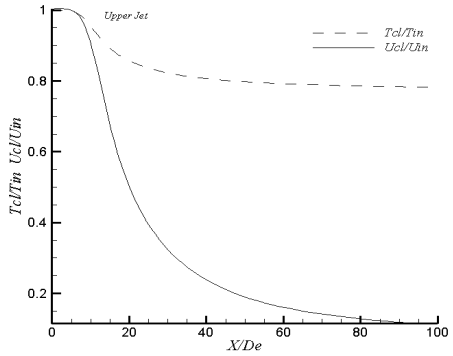

Fig 10 The centerline normalized velocity and temperature of upper jet

Fig. 11 shows the rate of variation of normalized entrainment flow along the jet. This parameter illustrates the strength of the large-scale mixing process. As it is shown in this figure the mass flow rate of about 21 times greater than the discharge flow rate is entrained into the jet over $x / D_e = 100$. In other words, the flow rate at $x / D_e = 100$ is 22 times greater than discharge flow rate. Mass entrainment is computed by the flux summation of cells located at the free boundaries.

The effects of Reynolds number on potential core of the upper and lower jets are shown in Table 2. By increasing the Reynolds number as it shown in this table, the potential core of jets increases. Due to increasing of Reynolds number while discharging momentum is constant, viscosity should be decreased, therefore turbulence intensity at the nearfield decreases and potential core increases by higher momentum.

Table 2
The effects of Reynolds number on potential core

Re	1000	5000	10000	50000
$X_{ci}\,upper / D_e$	2.36	2.57	2.64	2.72
$X_{ci}\,downer / D_e$	2.46	2.75	2.83	2.89

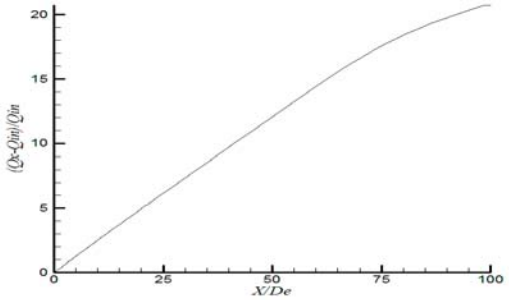

Fig. 11 Entrainment rate for Re = 5000, $H = 10D_e$

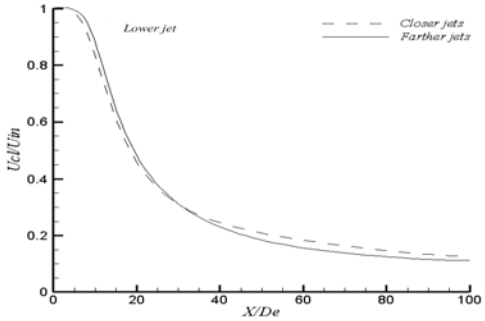

Fig. 12 Effects of distances between jets on velocity centerline

Changing the distances between jets has been considered by decreasing of distances to $H = 5D_e$ at the Re = 5000. Comparisons of entrained mass and velocity for different distance are shown in Figs. 12 and 13. It is seen from Fig. 12 that the jets at the nearfield, due to the closer distance of jet's centerlines, have more interaction and the closer jets spread faster than farther jets; but in the farfield, due to more mass entrainment from the free boundaries than closer jets, velocity centerline is higher at the farther jets. Consequently, large-scale mixing at the farther jets is more than closer while it is vice-versa for small-scale mixing. Mass entrainment decreases due to bring close jets as shown in Fig.13.

Changing the vertex angle of triangular jets for understanding how it affects on mixing parameters is important. In this research three different vertex angle of 30, 60 and 120 degrees at the Reynolds number of 5000 and $H = 10D_e$ are presented. Mass entrainment of these jets is compared with each other in Fig. 14. Equilateral triangular jet has more mass entrainment than isosceles, also its centerline velocity decreases faster than isosceles in the nearfield region. The potential core for isosceles is presented in Table 3. At the farfield all the jets are similar to each other and don't have significant differences and it is in agreement with previous experimental studies for different nozzles [4].

Table 3
The effects of vertex angle on potential core

Vertex angle (α)	30	60	120
$X_{ci}\,upper\,/\,D_e$	2.91	2.82	3.06
$X_{ci}\,downer\,/\,D_e$	3.05	2.93	3.15

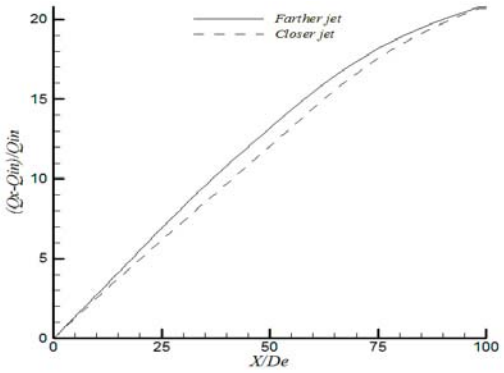

Fig. 13 Effects of distance between jets on mass entrainment

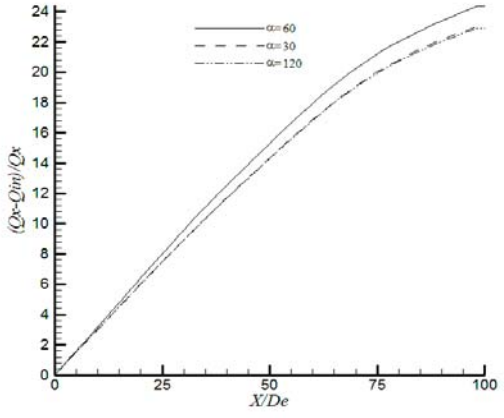

Fig. 14 Mass entrainment for different vertex angles

5. Conclusions

The sensitivity of an incompressible, turbulent free triangular jets flow to Reynolds number, distances between the jets and vertex angle conditions is numerically investigated. In this research effectiveness of $k-\varepsilon$ turbulence model for modeling of jets is examined with experiment and some of the specific conclusions are summarized as follows:

1. Industrial application of the jets such as internal combustion engines and reactors uses the array of nozzles and triangular nozzles combine the ability to obtain large-scale mixing in some geometry with the enhanced smallscale turbulent mixing in other geometries. This unique feature is important for the use in reactors where the large-scale mixing is required to get large amounts of the reactants together, while the small-scale mixing enhances the reaction rate by increasing the molecular contact.
2. It is found that due to the strong mixing of two jets their potential cores decrease and also mass entrainment is more than one triangular jet.
3. Secondary flow in planes that are vertical to symmetry causes flow from free boundary induces to domain. This induction at the vertex angle is more than triangular sides.
4. By increasing the Reynolds number at constant discharging momentum, the length of potential core increases. At the higher Reynolds, momentum difference of ambient and jet increases. Turbulence parameters and mixing entrainment are higher in low Reynolds and these are very important for combustion.
5. Temperature distribution is similar to velocity profiles but its potential core is lower than the potential core of velocity. This phenomenon shows that Reynolds thermal fluxes are stronger than its stresses.
6. Farther jets have stronger mixing than closer jets and mass entrainment decreases with increasing of distance between jets.
7. In general, relative to the one triangular jet, the centerline mean velocity of the jets decays more rapidly, implying increased entrainment of ambient fluid. Of particular interest is equilateral jets, which appears to produce the greatest mixing rates among all the jets investigated because of shorter potential cores.
8. Different inlet condition does not have major effects on the farfield while have great influence in nearfield.

References

1. **Abramovich, G.N.; Schindel, L.** 1963. The Theory of Turbulent Jets. The MIT Press.
2. **Rajaratnam, N.** 1976. Turbulent Jets. -New York: Elsevier Company.
3. **Mi, J.; Nathan, G.J.; Luxton. R.E.** 2000. Centreline mixing characteristics of jets from nine differently shaped nozzles. -Experiments in Fluids 28: 93-94.
4. **Xu, G.; Antonia, R.A.** 2002. Effect of different initial conditions on a turbulent round free jet, Exp. Fluids 33: 677-683.
5. **Quinn, W.R.** 1994. Development of a large-aspect-ratio rectangular turbulent free jet, AIAA J. 32: 547-554.

6. **Quinn, W.R.** 1995. Turbulent mixing in a free jet issuing from a low aspect ratio contoured rectangular nozzle, Aeronaut. J. 99: 337-342.
7. **Quinn, W.R.** 2005. Measurements in the near flow field of an isosceles triangular turbulent free jet, Experiment in Fluids 39: 111-126.
8. **Schadow, K.C.; Gutmark, E.; Parr, D.M.; Wilson, K.J.** 1988. Selective control of flow coherence in triangular jets, Experiments in Fluids 6: 129-135.
9. **Miller, R.S.; Madnia, C.K.; Givi, P.** 1995. Numerical simulation of non-circular jets, -J. Computers and Fluids 24: 1-25.
10. **Quinn, W.R.** 1990. Mean flow and turbulence measurements in a triangular turbulent free jet, I. J. Heat and Fluid Flow 11: 220-224.
11. **Bardow, A.; Bischof, C.H.; Bücker, H.M.; Dietze, G.; Kneer, R.; Leefken, A.; Marquardt, W.; Renz, U.; Slusanschi, E.** 2008. Sensitivity-based analysis of the $k-\varepsilon$ model for the turbulent flow between two plates, Chemical Engineering Science 63: 4763-4775.
12. **Benhamza, M.E.; Belaid, F.** 2009. Computation of turbulent channel flow with variable spacing riblets, Mechanika 5(79): 36-41.
13. **Wang, S.J.; Mujumdar, A.S.** 2005. A comparative study of five low Reynolds number k-ε models for impingement heat transfer, Applied Thermal Engineering 25: 31-44.
14. **Patankar, S.V.** 1980. Numerical heat transfer and fluid flow. New York: Hemispher.
15. **Peric, M.; Kessler, R.; Scheuerer, G.** 1988. Comparison of finite-volume numerical methods with staggered and collocated grids, J. Computers and Fluids 16: 389-403.
16. **Van Leer, B.** 1974. Towards the ultimate conservative difference-scheme. 2. Monotonocity and conservation combined in a second order scheme, J. Computational Physics 14: 361-370.
17. **Leonard, B.P.** 1979. A stable and accurate convective modeling procedure based on quadratic upstream interpolation, Comput. Meth. Appl. Mech. Eng. 19: 59-98.
18. **Zhou, X.; Sun, Z.; Brenner, G.; Durst, F.** 2003. Combustion modeling of turbulent jet diffusion H2/air flame with detailed chemistry, I.J Heat and Mass Transfer 43: 2075-2088.
19. **Zhou, X.; Sun, Z.; Brenner, G.; Durst, F.** 1999. Numerical Simulation of turbulent jet flow and combustion, I.J. Computers and Mathematics with Applications 38: 179-191.
20. **Schadow, K.C.; Gutmark, E.; Parr, D.M.; Wilson, K.J.** 1988. Selective control of flow coherence in triangular jets, Experiments in Fluids 6: 129-135.

I. Chitsaz, B. Farhanich

DVIEJŲ TRIKAMPIŲ KARŠTO SKYSČIO ČIURKŠLIŲ DINAMIKOS TYRIMAS

R e z i u m ė

Atliktas trikampių karšto skysčio čiurkšlių charakteristikų skaitinis imitavimas. Pateikti lygiakraščių ir lygiašonių tūtų trijų matmenų čiurkšlių, esant skirtingiems Reinoldso skaičiams ir atstumams tarp čiurkšlių, erdviniai rezultatai. Svarbiausiųjų lygčių sistema pritaikyta nustatytoms ribinėms sąlygoms, yra išspręsta baigtinių tūrių metodu atitinkamai išdėstant tinklelį. SIMPLEC algoritmas buvo panaudotas slėgiui ir greičiui tirti ir svarbiausioms tekėjimo ir energijos lygybėms nustatyti. Turbulentiniams įtempiams aproksimuoti naudojamas $k-\varepsilon$ modelis. Parodyti greičio ir temperatūros laukai ir nustatytas jų silpnėjimo čiurkšlės ašyje greitis. Parodyti pagrindinis ir antrinis srovių greičio vektoriai. Taip pat nustatyta skirtingo vertekso kampų įtaka trikampio skerspjūvio čiurkšlių maišymuisi. Šiame darbe buvo tyrinėti vertekso kampai nuo 30 iki 120°. Gauti rezultatai parodė, kad čiurkšlė geriau suformuojama esant lygiakraščiam skerspjūviui. Ypač daug dėmesio skirta Reinoldso skaičiaus (paremto hidrauliniu skersmeniu), taip pat įtekėjimo sąlygų įtakai trikampės čiurkšlės kitimui. Čiurkšlės charakteristikos labai priklauso nuo tekėjimo sąlygų. Tekėjimo rezultatų grafikai rodo didelę laisvų čiurkšlės ribų įtaką maišymui ir tekėjimui. Palyginti su viena trikampe čiurkšle, laisvas skysčio masės tiekimas šiuo atveju padidėja, o potenciali aktyvioji zona sumažėja.

I. Chitsaz, B. Farhanieh

NUMERICAL INVESTIGATION OF THERMO-FLUID DYNAMICS OF TWO TRIANGULAR JETS

S u m m a r y

This paper addresses the numerical simulation of thermo-fluid characteristics of triangular jets. The results of spatially developing, three dimensional jets from isosceles and equilateral nozzles at different Reynolds numbers and distances between jets are presented. The system of governing equations, subject to the proper boundary conditions is solved with the finite volume method with collocated grid arrangement. SIMPLEC algorithm was used for the pressure–velocity coupling to discrete the governing equations of flow and energy. The turbulent stresses are approximated using $k-\varepsilon$ model. The velocity and temperature fields are presented and rates of their decay at jet centerline are noted. The velocity vectors of main flow and secondary flow are illustrated. Also, the effect of different vertex angles on mixing in triangular cross-section jets is considered. The vertex angles that were considered for this work were 30 to 120 degree. The results showed that the jet entrains more with equilateral cross sections. Special attention has been drawn to the influence of the Reynolds number (based on hydraulic diameter) as well as the inflow conditions on the evolution of the triangular jet. The inflow conditions have considerable influence on the jet characteristics. The flow pattern results show strong mixing and flow entrainment from free boundaries into the jet. In comparison with single triangular jet mass entrainment from free boundaries is larger and also potential core is smaller.

И. Цхитсаз, Б. Фарханисх

ИССЛЕДОВАНИЕ ДИНАМИКИ ДВУХ ТРЕУГОЛЬНЫХ СТРУЙ НАГРЕТОЙ ЖИДКОСТИ

Р е з ю м е

В настоящей статье осуществляется числовая имитация характеристик треугольных струй нагретой жидкости. Представлены пространственные результаты равнобедренного и равностороннего сопел струи трех размеров при разных числах Реинольдса и расстоянии между ними. Система главных уравнений составлена для соответствующих предельных условий решена методом конечных объемов с соответствующим расположением сетки. SIMPLEC алгорифм использован при исследовании давления и скорости при определении главных уравнений течения и энерии. Турбулентные напряжения аппроксимировались при помощи $k–\varepsilon$ модели. Представлены поля скорости и температуры и определена скорость их уменьшения на оси струи. Показаны основной и вторичный векторы скоростей потока. Также определено влияние разных углов вертекса на смешивание в струях треугольного сечения. В этой работе исследовались углы вертекса от 30 до 120°. Результаты показали, что струя формируется лучше при равнобедренном сечении. Особое внимание обращено на влияние числа Рейнольдса (основанного на гидравлическом диаметре), а также условия входа на эволюцию треугольной струи. Условия входа имеют большое значение на характеристики струи. Графики результатов течения показывают большое значение свободных пределов струи на процесс смешивания и течения. По сравнению с одной треугольной струей в этом случае подача жидкости при свободных пределах возрастает, а потенциальная активная зона уменьшается.

Received September 23, 2010
Accepted April 11, 2011